PII: S0955-2219(98)00221-0

Characterization of $Nd_{1-x}Sr_xMnO_{3\pm\delta}$ SOFC Cathode Materials

G. Ch. Kostogloudis* and Ch. Ftikos

Laboratory of Inorganic Materials Technology, Department of Chemical Engineering, National Technical University of Athens, 9 Heroon Polytechniou Str., Zografou Campus, GR-157 80 Athens, Greece

Abstract

The crystal structure, thermal expansion behavior and electrical conductivity of $Nd_{1-x}Sr_xMnO_{3\pm\delta}$ ($x = 0$–0.5) perovskite oxides were investigated. The chemical compatibility of the compositions with 40 and 50 mol% Sr with Gd_2O_3 doped CeO_2 (CGO) electrolyte was also studied. An orthorhombic $GdFeO_3$-type symmetry (space group Pbnm, $z = 4$) was identified for all perovskite oxides, and the lattice parameters were determined. As the level of Sr doping increases, the pseudo-cubic lattice constant decreases, and the thermal expansion coefficient increases. The electrical conductivity can be described by the small polaron hopping conductivity model. The conductivity increases on increasing Sr doping, while the activation energy decreases. The compositions with 40 and 50 mol% Sr show very good thermal expansion and chemical compatibility with CGO electrolyte and can be considered as candidate intermediate temperature solid oxide fuel cell cathode materials. © 1999 Elsevier Science Limited. All rights reserved

Keywords: fuel cells, electrical conductivity, thermal expansion, CeO_2.

1 Introduction

In recent decades much effort has been directed towards solid oxide fuel cell (SOFC) development. A SOFC is an energy conversion device that produces electricity and heat by electrochemical combination of a fuel with an oxidant (air).[1] Its major advantages are: high efficiency, potential for cogeneration, modular construction, and very low pollutant emissions. The incorporation of a solid

electrolyte has the additional advantage that many problems associated with liquid electrolytes such as corrosion, flooding or electrode distribution may be overcome.[2]

SOFCs can be designed to operate over a wide range of temperatures: 500–1000°C. For high temperature operation (850–1000°C) there is a general agreement on the use of yttria stabilized zirconia (YSZ) solid electrolyte. Supported YSZ may be used down to 700°C. For lower temperatures, however, the use of YSZ is not appropriate, as its oxide ion conductivity is substantially reduced.[3] Doped CeO_2 electrolytes are considered more promising for operation at the intermediate temperature region of 500–700°C.[3,4] The ionic conductivity of $Ce_{0.9}Gd_{0.1}O_{1.95}$ (CGO) is about one order of magnitude higher than that of YSZ.[5] Despite its good conductivity, doped CeO_2 cannot be used at high temperatures, as its ionic transference number decreases drastically under the reducing atmosphere of the anode. A major advantage in using ceria-based electrolytes in the intermediate region is their excellent thermal expansion compatibility with ferritic stainless steel interconnect.[2]

An issue of high importance in SOFC technology, is the selection of appropriate ceramic electrocatalysts for the cathode electrode. The cathode must meet certain requirements, such as high electronic and oxide ion conductivity, high catalytic activity for oxygen reduction, chemical as well as thermal expansion compatibility with the electrolyte, no destructive phase transition within the operating temperature range, and controllable sintering behavior.[6] The most promising materials are the mixed conducting perovskite oxides of the structure ABO_3, where A and B are rare earth and transition metals respectively. $La_{0.84}Sr_{0.16}MnO_3$ is a well characterized cathode for the high temperature SOFC.[6] For operation at 700°C, Sr-doped lanthanum manganite on YSZ electrolyte[7] and $La_{0.6}Sr_{0.4}Co_{0.2}Fe_{0.8}O_{3-\delta}$ on CGO electrolyte[8,9] have

*To whom correspondence should be addressed. Fax: +30-1-772-3244; e-mail: gkostog@contral.ntua.gr

been successfully tested. However, alternative perovskite compositions incorporating other rare earth metals than La at the A-site, or other transition metals at the B-site have also been examined with the aim to improve the cathode performance.[10–12] It has been reported[10] that $Pr_{0.6}Sr_{0.4}MnO_3$ and $Nd_{0.6}Sr_{0.4}MnO_3$ have higher electrical conductivity and maintain lower overpotential values than $La_{0.6}Sr_{0.4}MnO_3$. Moreover, there is evidence that rare earth perovskites incorporating a smaller lanthanide cation than La^{3+} exhibit better chemical compatibility with the electrolyte.[13,14]

In this study, the crystal structure, thermal expansion behavior and electrical conductivity of $Nd_{1-x}Sr_xMnO_{3\pm\delta}$ ($x = 0$–0.5) were investigated. The effect of Sr content on the properties of this series of oxides is discussed. The chemical compatibility of selected compositions with CGO electrolyte was also examined, with the aim of their potential application in SOFCs operating at intermediate temperatures.

2 Experimental

Ceramic powders of the composition $Nd_{1-x}Sr_xMnO_{3\pm\delta}$ ($x = 0$–0.5) were prepared by the citrate synthesis and pyrolysis method.[15,16] Nd_2O_3 was dissolved in nitric acid, while $Sr(NO_3)_2$ and $(CH_3COO)_2Mn\cdot4H_2O$ were dissolved in water, all in the correct molar proportions. The exact amount of each metal in the respecting reagent had been determined by Atomic Absorption Spectroscopy (AAS), prior to the preparation of the solutions. The solutions were mixed together and an aqueous solution of citric acid, whose amount was that necessary to bind all the metals, was added. The final solution was heated over a burner flame until a viscous mass was obtained, followed by a large swelling. Combustion was then initiated, and subsequently pyrolysis took place. Finally, a fine homogeneous powder was obtained. The powder was calcined in air at 1100°C for 15 h, and then wet milled with acetone in a satellite-type milling apparatus using zirconia balls. After drying, the powders were compacted in the shape of cylindrical rods of approximate dimensions 50 mm length and 6 mm diameter, by cold isostatic pressing at 250 MPa. The compacts were then sintered in air at 1300°C for 15 h, and cooled to room temperature with a slow rate (1°C/min), to allow the equilibrium oxygen content to be established. The bulk densities of the sintered samples were measured by the Archimedes' method using distilled water as the liquid medium. In all cases densities above 94% of the theoretical values were obtained.

The structural study and the determination of the lattice parameters of the oxides were performed at room temperature by X-ray powder diffraction (XRD) on a Siemens diffractometer using CuK_α radiation. The diffractometer was operated at 40 kV and 30 mA. The XRD data were collected by step scanning in the range $10 \leq 2\theta \leq 80$ in increments of $0.02°$ 2θ. The lattice parameters were determined using a least squares unit cell refinement computer program (LSUCR).

The thermal expansion of the samples was measured in air using a dilatometer. The measurements were performed upon cooling in the temperature range from 800 to 100°C at a cooling rate of 5°C/min. The electrical conductivity was measured in air by the standard four point DC method upon heating in the temperature range 100–800°C at a heating rate of 5°C/min.

The samples for the chemical compatibility tests were prepared by mixing equimolar amounts of the perovskite and CGO electrolyte powders in an agate mortar using acetone. The mixtures were then dried, and pressed (250 MPa) in the shape of cylindrical pellets of 25 mm diameter. The pellets were subsequently sintered at 1300°C for 120 h. The temperature of 1300°C was selected for the chemical compatibility tests, because, although the operating temperature of the cell is substantially less, the fabrication of ceramic cathode/electrolyte/anode structures usually requires processing up to at least 1200°C.[4] The sintered pellets were milled, and then examined by XRD. The conditions of the measurements were the same as described above, but the angular range was this time limited to 20–35° 2θ, as the principal peaks of the possible reaction products, were expected to appear in this region.

3 Results and Discussion

3.1 Crystal structure
The X-ray powder diffraction patterns of the oxides in the system $Nd_{1-x}Sr_xMnO_{3\pm\delta}$ ($x = 0$–0.5) are shown in Fig. 1. In all cases single phase materials were obtained. The patterns were indexed on the basis of a distorted perovskite structure with orthorhombic $GdFeO_3$-type[17] symmetry (space group Pbnm). Each unit cell consists of four units, and has the approximate dimensions $\sqrt{2}a_p \times \sqrt{2}a_p \times 2a_p$, where a_p is the lattice parameter of the ideal cubic unit cell. The calculated lattice parameters and the volume of the unit cell are shown in Table 1.

As can be seen in Fig. 1, the splitting of the X-ray peaks in the case of the undoped neodymium manganite is large, indicating a severe distortion
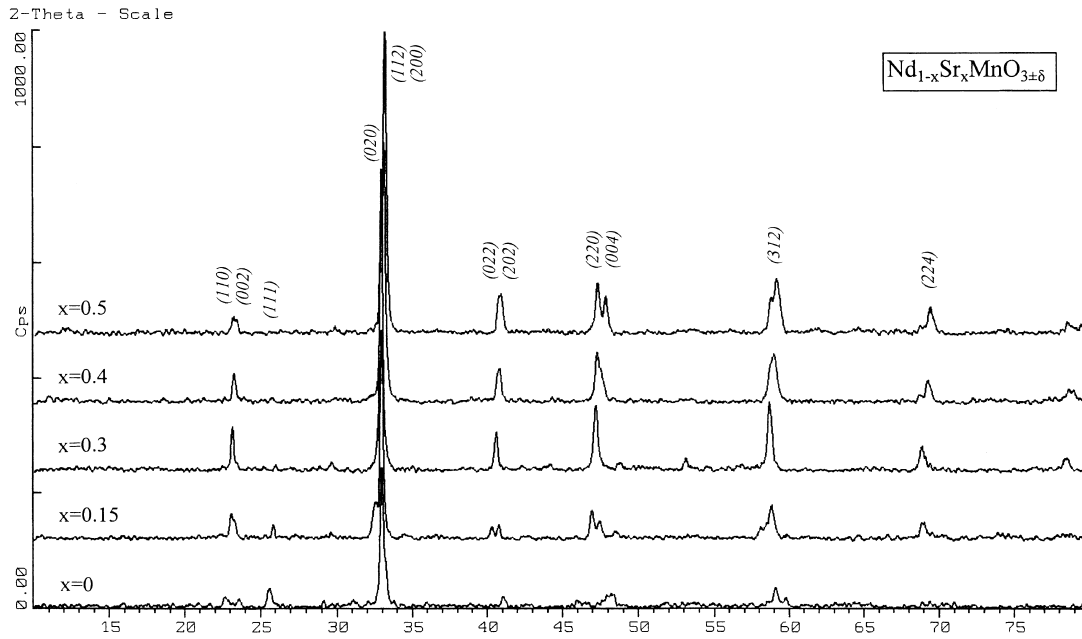
Fig. 1. X-ray powder diffraction patterns of $Nd_{1-x}Sr_xMnO_{3\pm\delta}$.

Table 1. Phase symmetry, lattice parameters, unit cell volume, orthorhombic deformation $D(\%)$, and type of orthorhombic structure of the system $Nd_{1-x}Sr_xMnO_{3\pm\delta}$

x (mol)	Phase symmetry	a (Å)	b (Å)	c (Å)	Volume (Å³)	c/√2 (Å)	a, b, c/√2 relation	Orthorhombic deformation D(%)	Type of orthorhombic structure
0	Orthorhombic	5·4067	5·6904	7·5378	231·9	5·3300	$c/\sqrt{2} < a < b$	2·60	O′-type
0·15	Orthorhombic	5·4346	5·5085	7·6588	229·3	5·4156	$c/\sqrt{2} < a < b$	0·68	O′-type
0·3	Orthorhombic	5·4396	5·4589	7·7171	229·2	5·4568	$a < c/\sqrt{2} \approx b$	0·15	O-type
0·4	Orthorhombic	5·4195	5·4680	7·6664	227·2	5·4210	$a \approx c/\sqrt{2} < b$	0·39	O-type
0·5	Orthorhombic	5·4275	5·4590	7·6260	226·0	5·3924	$c/\sqrt{2} < a < b$	0·42	O′-type

from the ideal cubic perovskite. This is caused by the relatively small size of Nd^{3+} cation, which is located at the center of the cubic cell. As a result, the MnO_6 octahedra are tilted and rotated to fill the extra space around the Nd^{3+} cation, causing the distortion. Goldschmidt[18] introduced a 'tolerance factor', t, as a measure of the deviation of ABO_3 structure from ideality:

$$t = \frac{r_A + r_o}{\sqrt{2}(r_B + r_o)} \qquad (1)$$

As t deviates from unity, the unit cell becomes more distorted. Considering Shannon's[19] ionic radii (Table 2) the tolerance factor for $NdMnO_3$ can be calculated as $t = 0.92$, assuming that Mn is

Table 2. Ionic radii of several ions, and their coordination number (CN) in the perovskite lattice[19]

Cation	Ionic radius (Å)
Nd^{3+} (CN = 12)	1·27
Sr^{2+} (CN = 12)	1·44
Mn^{3+} (CN = 6)	0·645
Mn^{4+} (CN = 6)	0·530
O^{2-} (CN = 6)	1·40

in the trivalent state. Actually, this is an approximation, since it is known that a small fraction of Mn ions exists in the tetravalent state at $pO_2 = 0.21$, due to the appearance of oxygen excess and cation vacancies,[20–23] according to the defect reaction:

$$6Mn_{Mn}^{\times} + \frac{3}{2}O_2 \Longleftrightarrow V_{Nd}''' + V_{Mn}''' + 6Mn_{Mn}^{\cdot} + 3O_O^{\times}$$
$$(2)$$
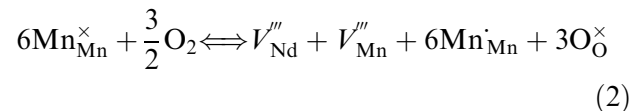
where Kroger–Vink notation[24] is used. The value of t can be increased (resulting in a decrease of distortion) by increasing the size of the A-site cation, and/or by decreasing the size of the B-site cation. When Sr^{2+} is introduced at Nd^{3+} lattice positions, electronic charge compensation is maintained by the oxidation of Mn^{3+} to Mn^{4+} cations:

$$SrMnO_3 \xrightarrow{NdMnO_3} Sr_{Nd}' + Mn_{Mn}^{\cdot} + 3O_O^{\times} \qquad (3)$$
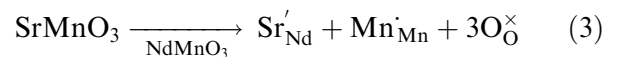
The larger size of Sr^{2+} cations compared to that of Nd^{3+}, and in addition the smaller Mn^{4+} cations compared to Mn^{3+}, cause t to increase and the

unit cell to come closer to ideality. This is supported by the results of Fig. 1, where the characteristic splitting of the X-ray peaks, gradually vanishes on Sr-doping. The composition with 30 mol% Sr appears to be the most symmetric, while when x increases further, the peaks split again (this is more noticeable for $x = 0.5$). It seems that the presence of the significantly larger Sr^{2+} cation compared to Nd^{3+}, at the A-site, enhances the distortion of the heavily doped neodymium manganites.

The relation among the lattice parameters, a, b, $c/\sqrt{2}$, can provide a measure of the distortion of the unit cell. This relation is included in Table 1. Generally, two types of orthorhombic structures are distinguished. The O-type structure, which is characterized by the relationship $a \leq c/\sqrt{2} \leq b$, exists when the lattice deformation is relatively small, while the O′-type structure, with $c/\sqrt{2} \leq a \leq b$, exists in the case of enhanced lattice deformation. As can be noticed, the structure of $Nd_{1-x}Sr_xMnO_{3\pm\delta}$ is O′-type for $x = 0$, 0.15, 0.5, and O-type for $x = 0.3$, 0.4. These results agree with those derived from the visual observation of the XRD patterns.

In order to quantitatively express the macroscopic distortion relative to the ideal perovskite structure, the quantity D (% orthorhombic deformation) is defined as:[25]

$$D = \frac{1}{3}\sum_{i=1}^{3}\left|\frac{a_i - \bar{a}}{\bar{a}}\right| \times 100 \qquad (4)$$

where $a_1 = a$, $a_2 = b$, $a_3 = c/\sqrt{2}$, and $\bar{a} = (abc/\sqrt{2})^{1/3}$. The values of D, calculated for each compound, are listed in Table 1. The evolution of the lattice parameters, as well as of D for comparison, are illustrated in Fig. 2 as x increases from $x = 0$ to 0.5. It can be seen that D is large in the case of the undoped compound, caused primarily by the high
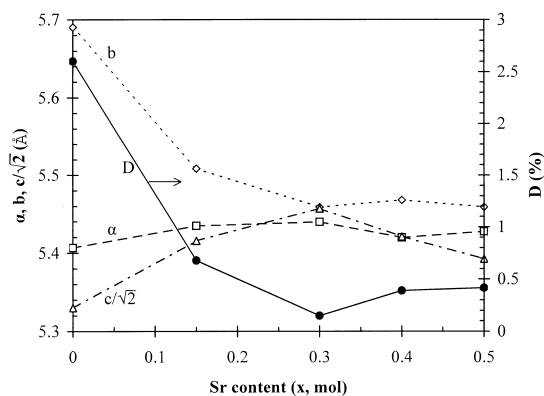
value of the parameter b. The increase of the Sr dopant concentration results in the decrease of D, which reaches its smallest value at $x = 0.3$, when the lattice parameters have very close values. Further increase of x causes D to increase again, due to the increase of the deviation among the lattice parameters.

To illustrate the effect of Sr doping on the size of the unit cell, the pseudo-cubic lattice constant (a') is defined as the cube root of the unit cell volume per ABO_3 unit:

$$a' = (V/z)^{1/3} \qquad (5)$$

where $z = 4$ for the oxides of this study. The values of a' are drawn in Fig. 3 as a function of Sr content. As can be seen, a' decreases as x increases. The change in the size of a' depends on factors such us the difference of ionic radius of the dopant cation (Sr^{2+}) in relation to the host cation (Nd^{3+}), as well as the ionic radii difference between the two oxidation states of the transition metal. In the case of $Nd_{1-x}Sr_xMnO_{3\pm\delta}$, a' tends to increase due to the substitution of the larger Sr^{2+} cation for Nd^{3+}. However, as Sr content increases, more Mn^{3+} cations are oxidized to form Mn^{4+}, according to eqn (3). So, a' tends to decrease, due to the smaller size of Mn^{4+} cations. Considering the radii of the ions involved (Table 2), it can be seen that the relative decrease of a' due to Mn oxidation is greater than its relative increase due to Sr^{2+} substitution. Therefore, a net decrease in the size of a' is expected to take place on Sr doping in neodymium manganite. This behavior has been previously reported for other rare earth manganites, too.[26–28] In the case of cobaltites,[29] however, where a small difference between the ionic radii of the two oxidation states of Co exists, the increase due to the incorporation of the larger Sr^{2+} cation at the A-site prevails, causing the net increase of a' as x increases. Another factor which is believed to contribute to the observed a' decrease on
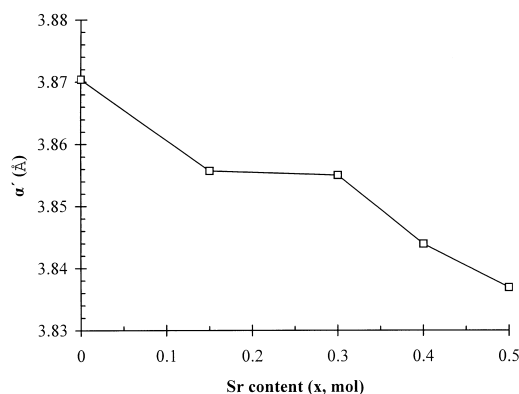

Fig. 2. Room temperature lattice parameters (a, b, $c/\sqrt{2}$) and orthorhombic deformation (D, %) of $Nd_{1-x}Sr_xMnO_{3\pm\delta}$ as a function of Sr content (x, mol).

Fig. 3. Pseudo-cubic lattice constant (a') as a function of Sr content (x, mol).

increasing x, in the oxides of this study, can be derived considering Pauling's second rule, concerning bond strength.[30] According to this rule, the formation of the tetravalent Mn ions is expected to strengthen the Mn–O bonds in MnO_6 octahedra. As a result, the size of MnO_6 octahedra and the volume of the perovskite unit cell decrease.

3.2 Thermal expansion

The linear thermal expansion curves of $Nd_{1-x}Sr_xMnO_{3\pm\delta}$, ($x = 0$–$0.5$) are shown in Fig. 4. For $x = 0$, the thermal expansion curve exhibits a break in the temperature range 600–750°C. A similar break was observed for $PrMnO_3$,[27] but in that case it was located at a lower temperature range (350–550°C). The appearance of a break in the thermal expansion curve of these oxides is attributed to a structure transition, and it is in agreement with the results of the electrical conductivity measurements, discussed in the next section.

As can be seen in Fig. 4, the thermal expansion curves of the Sr-doped compositions are linear, but they become steeper at high temperatures. The change of slope, which occurs at approximately 550–600°C, can be explained considering the temperature dependence of the defect structure of $Nd_{1-x}Sr_xMnO_{3\pm\delta}$. At room temperature, in air ($pO_2 = 0.21$), the undoped compounds, as well as those with low Sr content, show oxygen excess as a result of vacancies located at cation sites. These vacancies are considered to be randomly distributed at Nd and Mn sites in equal amounts.[21,23] With increasing temperature, the excess oxygen concentration (δ) in $Nd_{1-x}Sr_xMnO_{3+\delta}$ is reduced, and the equilibrium:
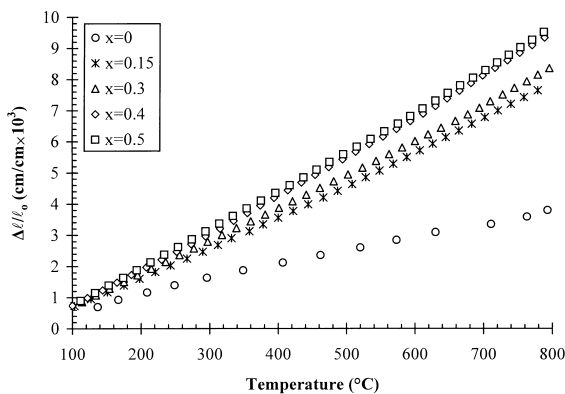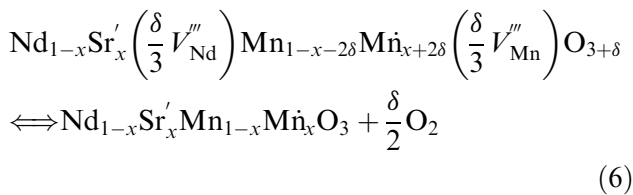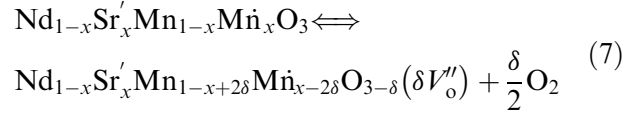
$$Nd_{1-x}Sr'_x\left(\frac{\delta}{3}V'''_{Nd}\right)Mn_{1-x-2\delta}\dot{M}\dot{n}_{x+2\delta}\left(\frac{\delta}{3}V'''_{Mn}\right)O_{3+\delta}$$

$$\Longleftrightarrow Nd_{1-x}Sr'_xMn_{1-x}\dot{M}\dot{n}_xO_3 + \frac{\delta}{2}O_2$$

$$(6)$$

shifts to the right. As a result, Mn^{4+} cations are reduced to form Mn^{3+}. For constant temperature, an increase in the Sr content causes the decrease of oxygen excess.[21] So, when x is about 0.4 the oxides are nearly stoichiometric, and can become oxygen deficient at higher x values, even at low temperatures.[31] With increasing temperature at this high x compositional range, the oxygen deficiency is enhanced, and the equilibrium:

$$Nd_{1-x}Sr'_xMn_{1-x}\dot{M}\dot{n}_xO_3 \Longleftrightarrow$$

$$Nd_{1-x}Sr'_xMn_{1-x+2\delta}\dot{M}\dot{n}_{x-2\delta}O_{3-\delta}\left(\delta V''_o\right) + \frac{\delta}{2}O_2 \quad (7)$$

shifts to the right. The result again is the reduction of Mn^{4+} to Mn^{3+}. Thus, it can be seen that irrespective of the level of Sr doping, the reduction $Mn^{4+}\rightarrow Mn^{3+}$ takes place when the temperature is increased. This is also confirmed by the results of Teraoka *et al.*,[32] who reported that in $La_{1-x}Sr_xMnO_{3\pm\delta}$, oxygen desorption takes place concurrently with $Mn^{4+}\rightarrow Mn^{3+}$ reduction, and the onset temperature for this desorption is 500°C. Furthermore, the temperature of thermal reduction $Mn^{4+}\rightarrow Mn^{3+}$ of MnO_2 oxide is known to be 535°C.[33] These temperatures are in good agreement with the temperature (550–600°C) where the change of slope in the thermal expansion curves of the oxides of this study takes place. Considering the ionic radii of the two oxidation states of Mn, a lattice expansion is expected to occur, when the concentration of Mn^{3+} ions is increased. In addition, the reduction of the manganese cations causes a decrease in the Mn–O bond strength according to Pauling's second rule,[30] and hence the size of MnO_6 octahedra increases, thus enhancing the lattice expansion.

The linear thermal expansion coefficients (TEC) were calculated from the slopes of the thermal expansion curves of Fig. 4 by linear regression, and they are drawn in Fig. 5 as a function of Sr content
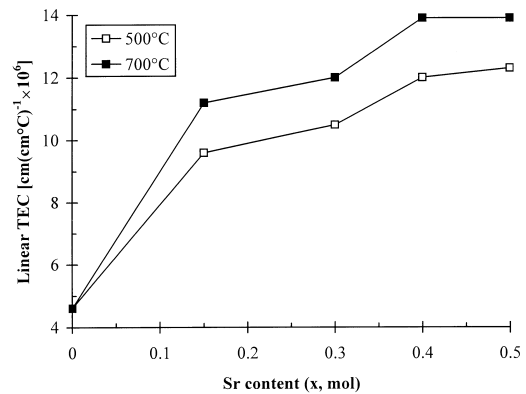

Fig. 4. Linear thermal expansion curves for $Nd_{1-x}Sr_xMnO_{3\pm\delta}$ in air.

Fig. 5. Linear thermal expansion coefficient (TEC) of $Nd_{1-x}Sr_xMnO_{3\pm\delta}$ at 500 and 700°C as a function of Sr content (x, mol) in air.

at 500 and 700°C (the operating temperatures of the intermediate temperature SOFC). It can be seen that the TEC values at 700°C are greater than those at 500°C, as a result of the change in the slope of the thermal expansion curves at around 550–600°C. At 500°C, the compositions with 40 and 50 mol% Sr, which have TEC values of 12×10^{-6} cm (cm°C)$^{-1}$ and 12.3×10^{-6} cm (cm°C)$^{-1}$, respectively, exhibit excellent thermal expansion compatibility with doped-CeO_2 electrolyte [TEC $= 12.5 \times 10^{-6}$ cm (cm°C)$^{-1}$]. At 700°C, both 40 and 50 mol% Sr-containing compositions have a TEC equal to 13.9×10^{-6} cm (cm°C)$^{-1}$, which is about 11% greater than that of doped-CeO_2 electrolyte. The magnitude of this thermal expansion mismatch, however, is acceptable and would not constitute a problem for the successful operation of the cell.

As can be seen in Fig. 5, for both 500 and 700°C, TEC increases with increasing Sr content. The same trend has also been observed in the case of other rare earth manganites.[26–28] According to the theory of thermal expansion developed by Ruffa,[34,35] the TEC is inversely proportional to the nearest neighbor distance r_n, which can be approximated to the metal-oxide ion bond length. Since in the ABO_3 perovskite lattice, the A–O distance is increased and the B–O distance is decreased when Sr is substituted for Nd at the A-site, it is more convenient to approximate r_n to half the pseudo-cubic lattice constant ($a'/2$). Therefore, the observed increase of the TEC can be explained considering the decrease of a' with increasing Sr content (Fig. 3). For $Pr_{1-x}Sr_xCoO_{3-\delta}$,[29] the TEC was found to decrease on increasing x. However, in that case a' increases on increasing x, and so the same relation between a' and TEC applies for rare earth cobaltites, too.

3.3 Electrical conductivity

The logarithm of electrical conductivity (logσ) of $Nd_{1-x}Sr_xMnO_{3\pm\delta}$ for $0 \le x \le 0.5$, is shown in Fig. 6 as a function of reciprocal temperature. The conductivity increases with increasing temperature for all compositions. The curve for the undoped compound, however, shows a break, during which an abrupt increase of conductivity is noticed. The temperature range at which the break occurs in the electrical conductivity curve (550–750°C), coincides fairly well with that observed in the thermal expansion curve. Similar breaks have been reported for the electrical conductivity curves of other rare earth manganites,[27,36] and have been attributed to a structure transition. The transition extends over a rather wide temperature range and it is not so sharp as in the case of a first-order phase transition. The results of a high temperature
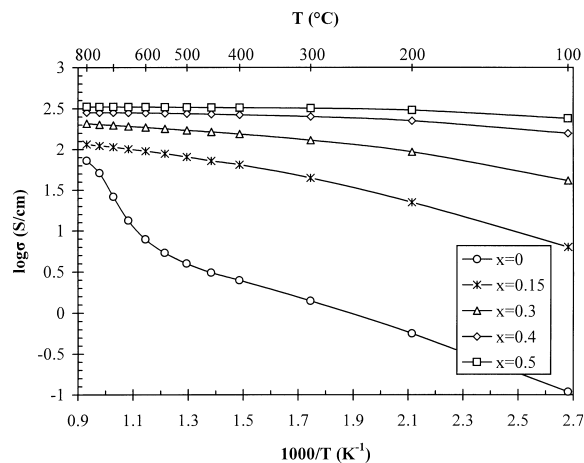

Fig. 6. Logσ versus reciprocal temperature (1000/T) for $Nd_{1-x}Sr_xMnO_{3\pm\delta}$ in air.

XRD study reported by Kamegashira et al.,[37] show that an orthorhombic-to-rhombohedral crystallographic transition occurs.

For all compositions, a semiconducting electrical behavior is observed (i.e. the conductivity increases with increasing temperature). In Fig. 7 it can be seen that there is a linear relationship between logσT and $1/T$, indicating that the conduction may be explained by the small polaron hopping mechanism. Indeed, the Mn^{4+} cations formed by Sr substitution [eqn (3)], as well as by the appearance of oxygen excess [eqn (2)], can be considered as p-type small polarons (holes). The difference in ionic radii between Mn^{4+} and Mn^{3+} cations (Table 2) produces a local distortion that can trap the charge at Mn^{4+} lattice positions.[38] Localization can occur when the bands are rather narrow, as it is believed is the case for the oxides of this study. Provided that sufficient energy is acquired, the polaron can hop among Mn sites, resulting in the observed semiconducting-type electrical conductivity behavior. Considering the classification scheme proposed by Day and Robin,[39,40] $Nd_{1-x}Sr_xMnO_{3\pm\delta}$ ($x = 0$–0.5) oxides can be classified to
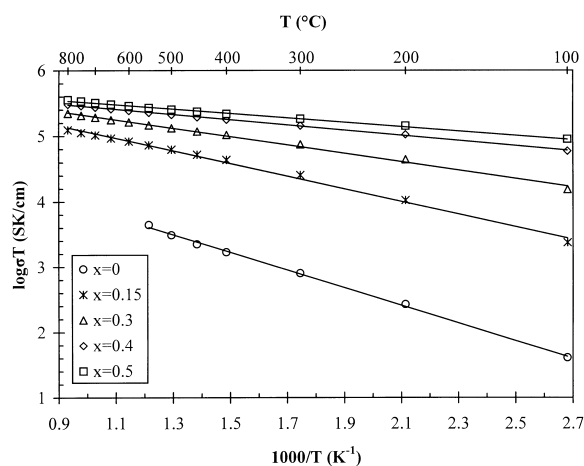

Fig. 7. LogσT versus 1000/T plots for $Nd_{1-x}Sr_xMnO_{3\pm\delta}$ in air.

class II mixed valency compounds. Class II compounds contain different environments for the two oxidation states, but there is enough interaction between them, so that polaron transfer, involving a small activation energy, is possible.

The temperature dependence of electrical conductivity through the small polaron hopping mechanism is expressed by:

$$\sigma = \frac{A}{T}\exp(-E_a/kT) \qquad (8)$$

The slope of the $\log\sigma T$ versus $1/T$ line gives the activation energy, E_a. The values of E_a calculated from the plots of Fig. 7 by linear regression, are given in Fig. 8. As can be seen, the activation energies range from 0.27 eV for the undoped composition, to 0.07 eV for the composition with 50 mol% Sr. These low E_a values are in agreement with the suggestion of a small polaron hopping conduction mechanism for the oxides in the system $Nd_{1-x}Sr_xMnO_{3\pm\delta}$. In Fig. 8 it can be noticed that E_a decreases as the level of Sr doping increases. The larger size of Sr^{2+} cation compared to Nd^{3+} (Table 2) brings the Mn–O–Mn angle closer to 180°. As a result, the orbital overlap between adjacent ions is increased. This overlap directly controls the interaction integral β, which is proportional to the width of the Mn–O bands.[41] The increase of the bandwidth results in the observed decrease of the activation energy.

As can be seen in Fig. 6, the conductivity increases with increasing Sr content for all temperatures within the examined temperature region. The substitution of Sr^{2+} for Nd^{3+} causes the oxidation of Mn^{3+} cations to Mn^{4+} for charge compensation reasons [eqn (3)]. As the Sr content increases, the concentration of Mn^{4+} charge carriers also increases, and higher electrical conductivity values can be achieved.
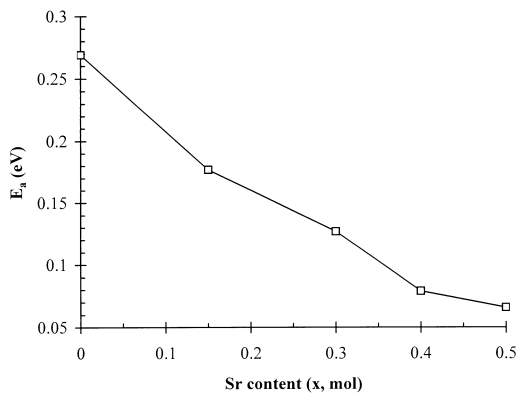
3.4 Chemical compatibility with $Ce_{0.9}Gd_{0.1}O_{1.95}$ electrolyte

The XRD patterns of the sintered (at 1300°C for 120 h) $Nd_{1-x}Sr_xMnO_{3\pm\delta}/CGO$ mixtures are shown in Fig. 9 for $x = 0.4$ and 0.5. These perovskite compositions were selected for the chemical compatibility tests, since they showed the best thermal expansion compatibility with CGO electrolyte. In both patterns, in the examined angular range of 20–35° 2θ, the peaks of the perovskite as well as of CGO can be observed, while no reaction products can be detected.

Chemical compatibility tests for $La_{1-x}Sr_x$ $MnO_{3\pm\delta}/YSZ$ mixtures, reported in the literature,[42,43] show that for 40 and 50 mol% Sr, the main reaction product is $SrZrO_3$. Also, the formation of $La_2Zr_2O_7$ as a minor product is reported for $x = 0.4$.[42] Considering these results, it could be expected that the main possible reaction product between $Nd_{1-x}Sr_xMnO_{3\pm\delta}$ ($x = 0.4$, 0.5) and CGO would be $SrCeO_3$, and possibly a small amount of $Nd_2Ce_2O_7$. However, the different radius ratios involved means that $Nd_2Ce_2O_7$ cannot be formed as a stable phase.[4] Moreover, although the formation of $SrCeO_3$ is possible, its stability is lower than that of $SrZrO_3$, because according to Yokokawa *et al.*[44,45] it has a smaller tolerance factor (*t*). Accordingly, $SrCeO_3$ can be considered as the main suspect reaction product for the compounds of this study, although its formation is expected to be suppressed compared to $SrZrO_3$. It is known that the principal XRD peak of $SrCeO_3$ is located at 29.4° 2θ. However, no peak is observed at this angular position, as Fig. 9 reveals. Thus, since no reaction products could be detected, it can be concluded that there is an excellent chemical compatibility between Sr-doped neodymium manganite and CGO solid electrolyte.
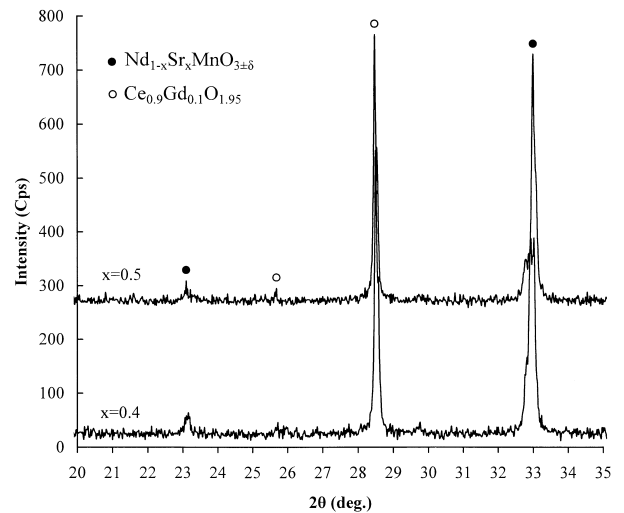

Fig. 8. Activation energy (E_a) for small polaron hopping conduction in the system $Nd_{1-x}Sr_xMnO_{3\pm\delta}$ as a function of Sr content (*x*, mol).

Fig. 9. XRD patterns of $Nd_{1-x}Sr_xMnO_{3\pm\delta}/Ce_{0.9}Gd_{0.1}O_{1.95}$ powder mixtures after sintering at 1300°C for 120 h. No reaction products were detected.

4 Conclusions

The oxides in the system $Nd_{1-x}Sr_xMnO_{3\pm\delta}$ ($x = 0$–0.5) have an orthorhombic $GdFeO_3$-type (space group Pbnm) perovskite structure. The undoped compound is severely distorted, but the increase of the level of Sr doping causes the tolerance factor to increase, which brings the unit cell closer to ideality. The composition with 30 mol% Sr is the most symmetric, while for higher x values the distortion seems to be enhanced. The pseudo-cubic lattice constant (a') decreases on increasing Sr doping, due to the oxidation of Mn^{3+} cations to the smaller Mn^{4+} cations. The thermal expansion curves are linear but they become steeper at high temperatures. The change of slope occurs at around 550–600°C, and it was attributed to a lattice expansion caused by the reduction $Mn^{4+}\rightarrow Mn^{3+}$, which takes place as the oxygen content decreases. The linear thermal expansion coefficient (TEC) increases on increasing Sr doping. This behavior was associated with the concurrent decrease of a'. The electrical conductivity of all compounds is semiconducting-type and can be described by the small polaron hopping conductivity model. The conductivity increases as the level of Sr content increases, due to the enhancement of Mn^{4+} charge carrier formation. The low activation energy (E_a) values are in agreement with the small polaron hopping mechanism. As x increases, E_a decreases, because the smaller Mn^{4+} cations formed, bring the Mn–O–Mn angle closer to 180°, thus increasing the bandwidth. The chemical compatibility of $Nd_{1-x}Sr_xMnO_{3\pm\delta}$ ($x = 0.4$, 0.5) with $Ce_{0.9}Gd_{0.1}O_{1.95}$ (CGO) electrolyte is excellent, since no reaction products were detected after 120 h of sintering of equimolar powder mixtures of these compounds at 1300°C. In addition, the TEC values of the perovskite compositions with 40 and 50 mol% Sr are compatible with that of CGO electrolyte, and therefore these compositions could be considered as candidate intermediate temperature SOFC cathode materials.

References

1. Minh, N. Q., *J. Am. Ceram. Soc.*, 1993, **76** 563.
2. Steele, B. C. H., *Phil. Trans. R. Soc. Lond. A*, 1996, **354**, 1695.
3. Steele, B. C. H., *Proceedings of the 14th Risø International Symposium on Materials Science: High Temperature Electrochemical Behaviour of Fast Ion and Mixed Conductors*, ed. F. W. Poulsen, J. J. Bentzen, T. Jacobsen, E. Skou and M. J. L. Østergård. Risø National Laboratory, Roskilde, Denmark, 1993, pp. 423.
4. Steele, B. C. H., *J. Power Sources*, 1994, **49**, 1.
5. Inaba, H. and Tagawa, H., *Solid State Ionics*, 1996, **83**, 1.
6. Hammou, A., *Advances in Electrochemical Science and Engineering*, ed. H. Gerischer and C. W. Tobias. VCH, Weinheim, Germany, 1992, Vol. 2, pp. 87.
7. Minh, N. Q., Kelly, P. and Montgomery, K., *Proceedings of the 2nd European SOFC Forum*, ed. B. Thorstensen. Switzerland, 1996, p. 659.
8. van Berkel, F. P. F., Christie, G. M., van Heuveln, F. H. and Huijsmans, J. P. P., *Solid Oxide Fuel Cells IV*, ed. M. Dockiya, O. Yamamoto, H. Tagawa and S. C. Singhal. The Electrochemical Society, Pennington, New Jersey, 1995, Vol. 95–1, pp. 1062.
9. Steele, B. C. H., Zheng, K., Rudkin, R. A., Kiratzis, N. and Christie M., *Solid Oxide Fuel Cells IV*, ed. M. Dockiya, O. Yamamoto, H. Tagawa and S. C. Singhal. The Electrochemical Society, Pennington, New Jersey, 1995, Vol. 95–1, p. 1028.
10. Ishihara, T., Kudo, T., Matsuda, H. and Takita, Y., *J. Electrochem. Soc.*, 1995, **142**, 1519.
11. Hrovat, M., Katsarakis, N., Reichmann, K., Bernik, S., Kuscer, D. and Holc, J., *Solid State Ionics*, 1996, **83**, 99.
12. Takeda, Y., Ueno, H., Imanishi, N., Yamamoto, O., Sammes, N. and Phillips, M. B., *Solid State Ionics*, 1996, **86**, 1187.
13. Subramanan, M. A., Aravamdam, G. and Subba Rao, G. V., *Prog. Solid State Chem.*, 1983, **15**, 55.
14. Uehara, T., Koto, K., Kanamaru F. and Horiuchi, H., *Solid State Ionics*, 1987, **23**, 137.
15. Baythoun, M. S. G. and Sale, F. R., *J. Mater. Sci.*, 1982, **17**, 2757.
16. Blank, D. H. A., Kruidhof, H. and Flokstra, J., *J. Phys. D,*, 1988, **21**, 226.
17. Geller, S., *J. Chem. Phys.*, 1956, **24**, 1236.
18. Goldschmidt, V. M., Skrifter Norske Videnskaps-Akad. Oslo. I. Mathemat. Naturwiss. Klasse No 8, 1926.
19. Shannon, R. D., *Acta Crystallogr.*, 1976, **A32**, 751.
20. Tofield, B. C. and Scott, W. C., *J. Solid State Chem.*, 1974, **10**, 183.
21. Kuo, J. H., Anderson, H. U. and Sparlin, D. M., *J. Solid State Chem.*, 1989, **83**, 52.
22. Cherepanov, V. A., Burkhatova, L. Yu., Petrov, A. N. and Voronin, V. I., *J. Solid State Chem.*, 1995, **118**, 53.
23. van Roosmalen, J. A. M., Cordfunke, E. H. P., Helmoldt, R. B. and Zandbergen, H. W., *J. Solid State Chem.*, 1994, **110**, 100.
24. Kruger, F. A., *The Chemistry of Imperfect Crystals*. North-Holland, Amsterdam, 1964.
25. Knizek, K., Jirak, Z., Pollert, E. and Zounova, F., *J. Solid State Chem.*, 1992, **100**, 292.
26. Hammouche, A., Siebert, E. and Hammou, A., *Mater. Res. Bull.*, 1989, **24**, 367.
27. Kostogloudis, G. Ch., Vasilakos, N. and Ftikos, Ch., *J. Eur. Ceram. Soc.*, 1997, **17**, 1513.
28. Kostogloudis, G. Ch. and Ftikos, Ch., *J. Mater. Sci.*, submitted for publication.
29. Kostogloudis, G. Ch., Vasilakos, N. and Ftikos, Ch., *Solid State Ionics*, 1998, **106**, 207.
30. Pauling, L., *The Nature of the Chemical Bond*. 3rd. edn. Cornell University Press, Ithaca, N.Y., 1960.
31. Mizusaki, J., Tagawa, H., Naraya, K. and Sasamoto, T., *Solid State Ionics*, 1991, **49**, 111.
32. Teraoka, Y., Yoshimatsu, M., Yamazoe, N and Seiyama, T., *Chem. Lett.*, 1984, 893.
33. Mukikagaku Handbook [Inorganic Chemistry Handbook], Chap.1. Gihodo Shuppan, Tokyo, 1981.
34. Ruffa, A. R., *J. Mater. Sci.*, 1980, **15**, 2258.
35. Ruffa, A. R., *J. Mater. Sci.*, 1980, **15**, 2268.
36. Kuo, J. H., Anderson, H. U. and Sparlin, D. M., *J. Solid State Chem.*, 1990, **87**, 55.
37. Kamegashira, N. and Miyazaki, Y., *Phys. Stat. Sol. A*, 1983, **76**, K39.
38. Cox, P. A., *The Electronic Structure and Chemistry of Solids*. Oxford University Press, Oxford, 1987.
39. Robin, M. B. and Day, P., *Adv. Inorg. Chem. And Radiochem.*, 1967, **10**, 247.
40. Day, P., *Int. Rev. Phys. Chem.*, 1981, **1**, 149.
41. Burdett, J. K., *Chemical Bonding in Solids*. Oxford University Press, Oxford, 1995.

42. van Roosmalen, J. A. M. and Cordfunke, E. H. P., *Solid State Ionics*, 1992, **52**, 303.

43. Stochniol, G., Syskakis, E. and Naoumidis, A., *J. Am. Ceram. Soc.*, 1995, **78**, 929.

44. Yokokawa, H., Sakai, N., Kawada T. and Dokiya, M., *J. Solid State Chem.*, 1991, **94**, 106.

45. Yokokawa, H., Kawada, T. and Dokiya, M., *J. Am. Ceram. Soc.*, 1989, **72**, 152.